Computers in Biology and Medicine 107 (2019) 248–256

Contents lists available at ScienceDirect

Computers in Biology and Medicine

journal homepage: www.elsevier.com/locate/compbiomed

Portable brain-computer interface based on novel convolutional neural network

Yu Zhang, Xiong Zhang*, Han Sun, Zhaowen Fan, Xuefei Zhong

Department of Electronic Science and Engineering, Southeast University, Nanjing, 210096, China

ARTICLE INFO

Keywords:
Brain-computer interface
Biomedical signal processing
Dry electrode
Convolutional neural network
Motor imagery

ABSTRACT

Electroencephalography (EEG) is a powerful, noninvasive tool that provides a high temporal resolution to directly reflect brain activities. Conventional electrodes require skin preparation and the use of conductive gels, while subjects must wear uncomfortable EEG hats. These procedures usually create a challenge for subjects. In the present study, we propose a portable EEG signal acquisition system. This study consists of two main parts: 1) A novel, portable dry-electrode and wireless brain–computer interface is designed. The EEG signal acquisition board is based on 24 bit, analog-to-digital converters chip and wireless microprocessor unit. The wireless portable brain computer interface device acquires an EEG signal comfortably, and the EEG signals are transmitted to a personal computer via Bluetooth. 2) A convolutional neural network (CNN) classification algorithm is implemented to classify the motor imagery (MI) experiment using novel feature 3-dimension input. The time dimension was reshaped to represent the first and second dimension, and the frequency band was used as the third dimension. Specifically, frequency domain representations of EEG signals obtained via wavelet package decomposition (WPD) are obtained to train CNN. The classification performance in terms of the value of kappa is 0.564 for the proposed method. The *t*-test results show that the performance improvement of CNN over other selected state-of-the-art methods is statistically significant. Our results show that the proposed design is reliable in measuring EEG signals, and the 3D CNN provides better classification performance than other method for MI experiments.

1. Introduction

Human–computer interfaces (HCIs) based on bioelectrical signals have received increasing attention over the last decade [1]. Common types of HCI bio-signals include electromyography, electroencephalography (EEG), electrooculography, and functional near-infrared spectroscopy [2]. EEG is one of the most common techniques. EEG is a method for measuring the electrical activity of the brain using electrodes placed on the scalp [3–5]. EEG is a noninvasive tool that can provide high temporal resolution to directly represent the dynamics of brain activities. EEG has been widely used for both medical diagnoses and neurobiological research. Recent research has opened up the possibility for its use in novel brain–computer interfaces (BCIs) focused on enhancing the performance of healthy users.

Traditionally data collection for EEG based BCIs uses wet Ag/AgCl electrodes that are uncomfortable and require considerable time to apply [6]. To improve the performance of conventional Ag/AgCl electrodes, gel-less electrodes has been designed. Gel-less electrodes include micro-needle, tips, spring pin, and soft conductive polymer. The most common candidate used for these needle array electrodes has been micromachined silicon needles, fabricated through wet-chemical etching methods and then coated with a biocompatible conducting coating. a micro-electro-mechanical system (MEMS) has been used with dry MEMS electrodes to measure EEG signals [7]. This dry electrode is designed to pierce the stratum corneum into the electrically conducting tissue layer stratum germinativum. Radhakrishnan has designed a needle array dry electrode, which has a 10*10 array of stainless steel microtips assembled over a Teflon base of 1 cm diameter [8]. MEMS electrodes can acquire EEG signals without conductive gels, but MEMS electrodes can't penetrate hair [9,10]. In addition to the needle electrode, noncontact capacitive electrodes can be used [11,12]. However, noncontact capacitive electrodes are affected by motion artifacts. other kind of dry electrode is made of conductive rubber [13,14], metal (just like iridium-oxide [15] or silver [16]) and polyurethanes(TPU) [17,18]. Some designe have been applied to brain computer interface. We think that the use of a metal dry electrode is also a good method.

* Corresponding author.
E-mail addresses: 230129600@seu.edu.cn (Y. Zhang), zxbell@seu.edu.cn (X. Zhang), hansun@seu.edu.cn (H. Sun), zhaowenfan@seu.edu.cn (Z. Fan), zxf@seu.edu.cn (X. Zhong).

https://doi.org/10.1016/j.compbiomed.2019.02.023
Received 4 November 2018; Received in revised form 26 February 2019; Accepted 26 February 2019

In the classification part, many traditional classifiers like support vector machine (SVM), linear discriminant analysis (LDA) [19], and k-nearest neighbor (k-NN) [20] that have been employed in research and pattern recognition techniques are utilized for EEG signal detection. Common spatial patterns (CSPs) are widely used in motor imagery (MI) tasks [21]. Other methods, like independent component analysis and principal component analysis (PCA) have been used to improve classification accuracy [19]. In recent years, many machine learning researchers have focused on deep neural networks, which have been improved with backpropagation neural networks, including deep belief networks (DBNs), restricted Boltzmann machines (RBMs), auto-encoders, convolutional neural networks (CNNs), and recurrent neural networks [22-27.].

CNN is artificial neural networks that can learn local patterns in data by using convolutions as their key component. CNN vary in the number of convolutional layers, ranging from convolutional layer such as in a successful handwritten recognition CNN [28] over deep CNN with multiple convolutional layers (5 convolutional layers and 3 full connection layers) [29] to very deep architectures with more than 1000 layers as in the case of the recently developed residual networks [30]. Now CNNs are also used in MI classification research [2]. Some research uses different methods to convert the EEG signal to an image representation before applying the CNN. In a report, Pouya et al. proposed a novel approach to learning such representations for a multi-channel EEG time series, and demonstrated its advantages in the context of a mental load classification task [31]. EEG activities were transformed into a sequence of topology-preserving multi-spectral images. In another report, Yang et al. proposed a frequency complementary feature map selection scheme by constraining the dependency between frequency bands [32]. Augmented common spatial pattern (ACSP) features were generated based on pair-wise projection matrices, which covered various frequency ranges. In some studies, the input form of CNN has 2-dimension, time dimension was first dimension, and the channel was second dimension [33–38]. Other studies used 2-dimension input form, but frequency was first dimension, and time was second dimension by Short Time Fourier Transform [39,40].

In this study, we design a wireless, portable EEG system based on dry EEG sensors, with an embedded system that prevents channel connection and fixation. We proposed a system with a small size of 3*4 cm, which was attached to headphones. Traditional BCI systems require the use of an EEG cap, however, the cap is uncomfortable. Thus, a headphone EEG was considered in the design of the proposed system. The subjects felt more comfortable with the headphones than with the EEG cap. We present a novel CNN to classify MI. we propose a new feature structure. The signal was reshaped to a 3-dimension matrix, the time dimension was reshaped to represent the first and second dimension, and the frequency band was used as the third dimension. The proposed method has achieved good performance on the motor imagery, and significantly increase the average accuracy.

The structure of this paper is as follows: Section 2 introduces the portable EEG acquisition system. Section 3 introduces the experimental methods and design. Signal processing and classification are discussed in Section 4. Section 5 describes the results of three experiments. Finally, Section 6 discusses and concludes the current work.

2. System architecture

2.1. Wireless acquisition system

Fig. 1 shows the wireless EEG acquisition system. The system was used to acquire EEG signals from dry sensors, and includes an Analog to Digital Converter (ADC) component, and a wireless microprocessor component.

The ADC used was an ADS1298 model (Texas Instruments), which is a family of multichannel, simultaneous sampling, 24 bit, analog-to-digital converters with built-in programmable gain amplifiers. The ADS19298 Delta–Sigma ADC is a device for biopotential measurements and medical instrumentation with eight low-noise, programmable gain amplifiers and high 24 bit resolution. Each channel has 0.75 mW power. The ADS1298 has a resolution of approximately 0.5 μV while the alpha (8–15 Hz) and beta (16–31 Hz) waves of an EEG have amplitudes of 1–50 μV. The device has self-test, temperature, and leadoff detection mechanisms. The max sample rate is 32 kSPS, the SNR is 112 DB, the common-mode rejection ratio (CMRR) is −115 dB, and the max programmable gain is 12.

The wireless microprocessor component used was the Nordic nRF51822, a highly flexible multi-protocol SOC for near-field communication that allows for the usage of multiple communication protocols on the same SOC. Implementation of such a highly flexible architecture allows system to be built by varying the combination of components themselves or by changing the configuration of existing components. The microprocessor transfers data to a host device (PC). The ADC are connected to the nRF51822 using a standard serial peripheral interface (SPI).

The proposed dry EEG sensors were in direct contact with the scalp surface with probes, as shown in Fig. 2. Each probe consisted of a head, spring, and sleeve. The probe head was copper, and its surface was gold-plated (Au). Au has excellent biocompatibility and does not produce adverse effects on human skin. To collect effective EEG signals over hair, the probe heads should be designed like a comb, and the hair should be able to pass between the probes without becoming trapped underneath and thereby preventing electrical contact with the scalp. The probe head was less than 0.7 mm in diameter, so the probes did not penetrate the skin. The probe was embedded into a sleeve made of copper (Cu); each sleeve was connected to a spring. This mechanism was designed to allow a feedback force of 10 g to act as a buffer for the probe when a force was applied to the dry sensors. The spring force must be large enough to ensure that the sensor attaches to the scalp surface and maintains the proper sensor–skin contact impedance quality, but the spring force must be small enough to ensure that the head does not penetrate the skin. Three probes were inserted into the PCB plate that served as a flexible plastic substrate for the sensor. After insertion, all the probes were connected together. When a force was applied to the sensor, the head of the sensor fit the scalp well. The spring contact probe and plastic substrate provided buffering, and the sensor could attach to the scalp well without pain. The plastic substrates were made with a 3D printer.

3. Methods

3.1. Subject

Seven able-bodied subjects (all subjects were male; mean age was 26.2 yrs) participated in the data acquisition. Two subjects had experience with EEG, and the other five subjects had no experience with EEG. All subjects signed the consent form approved by the Academic Ethics Committee of Southeast University before the experiments began. All subjects were university-educated and non-smoking, with no history of brain injuries or neurological disorders. Instructions for off-line and online feedback experiments were carefully explained and illustrated, and the first subjects were allowed some practice. During the experiments, subjects sat motionless in a comfortable chair and rested their hands on a desktop.

3.2. Acquisition setup

In the experiments, two sensors were placed at industry standard points C3 and C4 (for MI) or O1 and O2 (for visual alpha wave measurement). An illustration of these points is given in Fig. 3. The left earlobe is a reference point, and the right earlobe is a ground point. All systems were fixed to a headphone; Fig. 3 shows our easy-to-wear headphone EEG acquisition system (see Fig. 3).

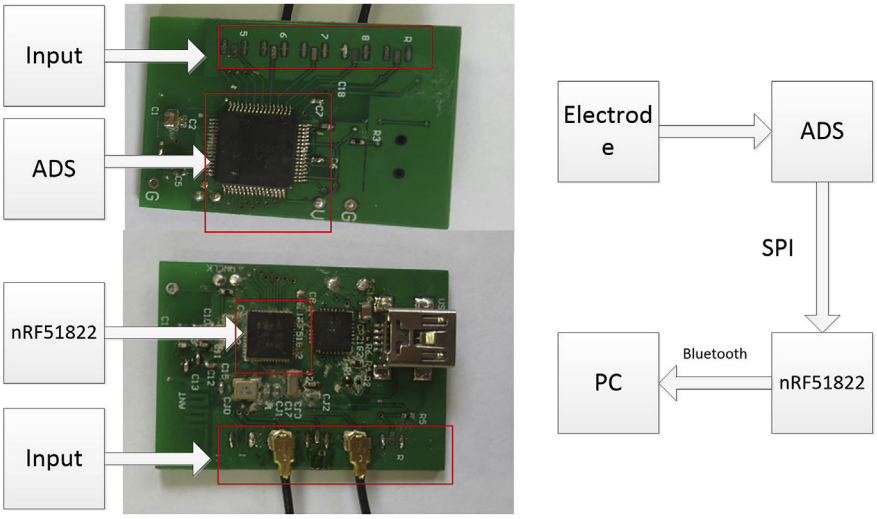

Fig. 1. PCB design, top and bottom of the board (left); EEG system board component integration view (right).

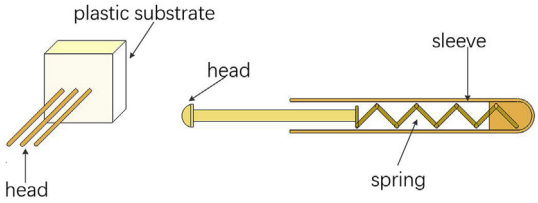

Fig. 2. Probe head, spring, and sleeve (right); a schematic design of the EEG sensor on the plastic substrate.

Placement: For MI experiment, first we need to find the location of CZ, one line was from nose to external occipital protuberance, another line was between ears (or more accurately, the concave in front of the ear), the cross point was CZ. The C3 and C4 is found halfway between CZ and ears. For alpha wave experiment, we know that alpha wave usually occupies the occipital electrodes. So we just put the electrodes in the occiput [41]. About gravity: the headphone is very light, and The headphone firmly clips the head.

3.3. Experimental protocol

3.3.1. Alpha wave experiment

A common technique for EEG recording system validation is the analysis of alpha waves [41]. Alpha waves were detected in the occipital lobe area (O1 and O2) when the subject was asked to close their eyes. We used two devices for data acquisition: one was an EEG acquisition system of our own design, and the other was the SynAmps2 system (Neuroscan Co., Ltd). The subject was asked to close their eyes for 20 s.

3.3.2. MI experiment

The MI experiment consisted of 10 runs of 40 trials each. All runs finished on the same day, with breaks of several minutes between runs. 400 trials of 9 s duration were run. The first 2 s were quiet, and then at t = 2 s an acoustic stimulus indicated the beginning of the trial. At t = 3 s, an arrow (left or right) was displayed as a cue. At the same time, the subject was asked to imagine left- or right-hand movements. Fig. 4 shows paradigm of MI experiments.

The feedback experiments were scheduled after a week of MI experiments. In the feedback experiments, the process was the same as in the MI experiments, but at t = 8 s, a result of CNN was shown on the screen, and subjects were told whether their imagery was right or

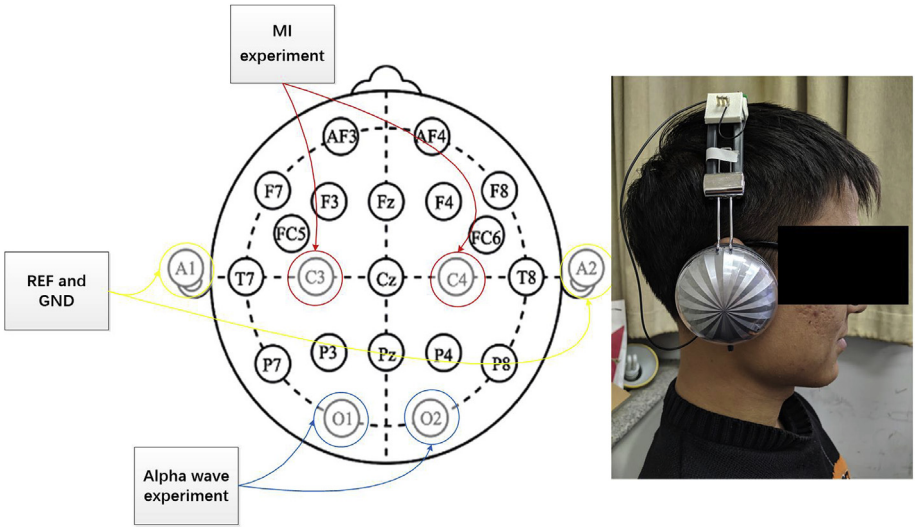

Fig. 3. 10–20 electrode system (left); EEG system fixed on a headphone (right).

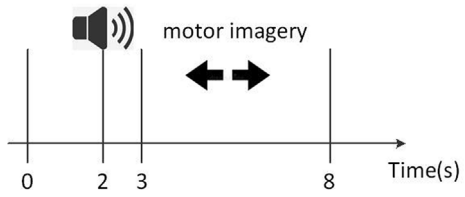

Fig. 4. Paradigm of MI experiments.

wrong. Four subjects (S1, S2, S3, and S6) participated in MI feedback experiments.

3.4. Signal preprocessing

All data processing was performed within MATLAB. In the beginning, we used an infinite impulse response (IIR) filter to remove noise. The band-pass frequency was from 0.5 to 100 Hz. Then the EEG signals were passed through a notch filter at 50 Hz. The subsequent step was feature extraction.

3.5. Feature extraction

The EEG signal contains information about various processes taking place in the brain, hence, it was essential to extract the EEG feature that was representative of MI alone. The feature of the EEG signal was extracted from the raw EEG. There have been further attempts to analyze EEG signals by investigating the different frequency band components separately, such as alpha (8–12 Hz) and beta (18–26 Hz) rhythms. The oscillatory power of the alpha rhythm in the sensorimotor cortex ipsilateral to the imagined tasks increased, while that of the beta rhythm in the contralateral sensorimotor cortex decreased simultaneously. In this study, we used wavelet packets to decompose the EEG signals. Wavelet packet decomposition has multi-resolution capability, which is appropriate for non-stationary EEG signals [42]. A seven-layer decomposition of the wavelet was implemented to extract the raw EEG signals (4–6 Hz), (6–8 Hz) … …(36–38 Hz), (38–40 Hz). The decomposition space tree and frequency ranges are shown in Fig. 5. The alpha rhythms consist of (8–10 Hz) and (10–12 Hz) bands, and beta rhythms consist of (18–20), (20–22), (22–24), and (24–26) bands. For the time of the feature, we cut the data to 0.5–4.5 s per trial. There were 1024 sample points per trial, at a sampling rate of 256 points per second. The sample points be transformed to 32*32. as shown in Fig. 5, so we obtained new data form. This data was a feature of the EEG.

3.6. Feature selection

The feature selection step can be applied after the feature extraction step to select a subset of features for the various potential benefits. Among the various features that one may extract from the EEG signals (feature extraction), some features may not be relatable to mental states through the BCI. The number of parameters that the classifier must optimize is positively correlated with the number of features. Reducing the number of features gives fewer parameters that must be optimized by the classifier. From the knowledge extraction perspective, if only a few features are selected and ranked, it is easier to observe which features are actually related to the targeted mental states. A model with fewer features can produce faster predictions for a new sample.

It has been shown that the energy in the alpha band observed in the motor cortex of the brain decreases when an MI task is performed. This decrease is called event-related desynchronization (ERD). An MI task also causes an energy increase in the beta band, which is called event-related synchronization (ERS). Left- and right-hand movement MI tasks are said to cause ERD and ERS, respectively, in the right and left sides of the motor cortex, affecting the EEG signals at the C3 and C4 electrodes [43]. In this paper, we selected alpha rhythms (8–12 Hz) and beta rhythms (18–26 Hz) as the frequency band [44,45].

3.7. Classification

The objective of BCI classification is to categorize according to SVM or k-NN, which are some of the common classifiers used for BCI research. In this paper, we use CNN classifiers [29].

CNN: Here we introduce a network—a compact CNN architecture for EEG-based BCIs. The network model can be found in Fig. 6 and Table 1. We have C channels and T time samples; C is 6 and T is 1024. We fit the model using the Adam optimizer, while minimizing the cross-entropy loss function. We ran 500 training iterations with validation stopping. All data were trained using an Nvidia GTX1060 GPU with CUDA9 in PyTorch.

This network has five layers, not including the input and output layers. The input is a 6@32*32 date (alpha rhythms is 2 and beta rhythms is 4), similar to a pixel image. In the following, we describe the details of each layer.

Layer L1 is a convolutional layer with 16 feature maps. Each filter is of 5*5 size. The activation function selected is a rectified linear unit (ReLU) function. The ReLU is approximated by a softplus function, defined as

$$a = W^T * X + b \tag{1}$$

$$\mathrm{F}(a) = max(0, a) \tag{2}$$

where x is the input, W is the weight matrix, and b is the bias value.

Layer L2 is a subsampling layer that uses max pooling with 16 feature maps of size 12*12. Max pooling is a sample-based discretization process. The objective is to down-sample an input representation (image, hidden-layer output matrix, etc.), reducing its dimension and allowing assumptions to be made about features contained in the binned sub-regions. The feature maps in L2 have half the number of rows and columns of L1.

Layer L3 is a convolutional layer with 32 feature maps. Each filter is of 5*5 size. The output function is a ReLU function, as in L1.

Layer L4 is a subsampling layer with 32 feature maps of size 8*8.

Layer L5 is a convolutional layer with 64 feature maps. Each filter is of 8*8 size. The output function is a ReLU function, as in L1.

Output: In the output layer, the features are passed directly to a softmax classifier. We used the dropout technique. We set the dropout probability to 50% to reduce overfitting.

Comparison with state-of-the-art methods: To evaluate the performance of 3D(3-dimension) CNN, comparison experiments have been conducted for CNN and other state-of-the-art methods, including deep belief networks (DBN) [27] and 2D(2-dimension) CNN [37]. The traditional methods in BCI, k-NN [46] and SVM [47], have been compared too.

4. Results

4.1. Alpha wave experiment

The Fourier transform of two signals was computed to obtain the power of the different frequencies, as shown in Fig. 7. The left signal is from electrode O1, and the right from O2. The blue line is acquired by Neuroscan; the red line is acquired by our devices. During the eyes-closed interval, increased activity in the 8.5–10 Hz region of the frequency domain indicated an alpha wave signal in the occipital lobe area [48].

4.2. MI experiment

The classifiers were trained and tested for each subject. The performance of the proposed method was evaluated using accuracy and mean kappa value. A total of 80% of trials were randomly selected for

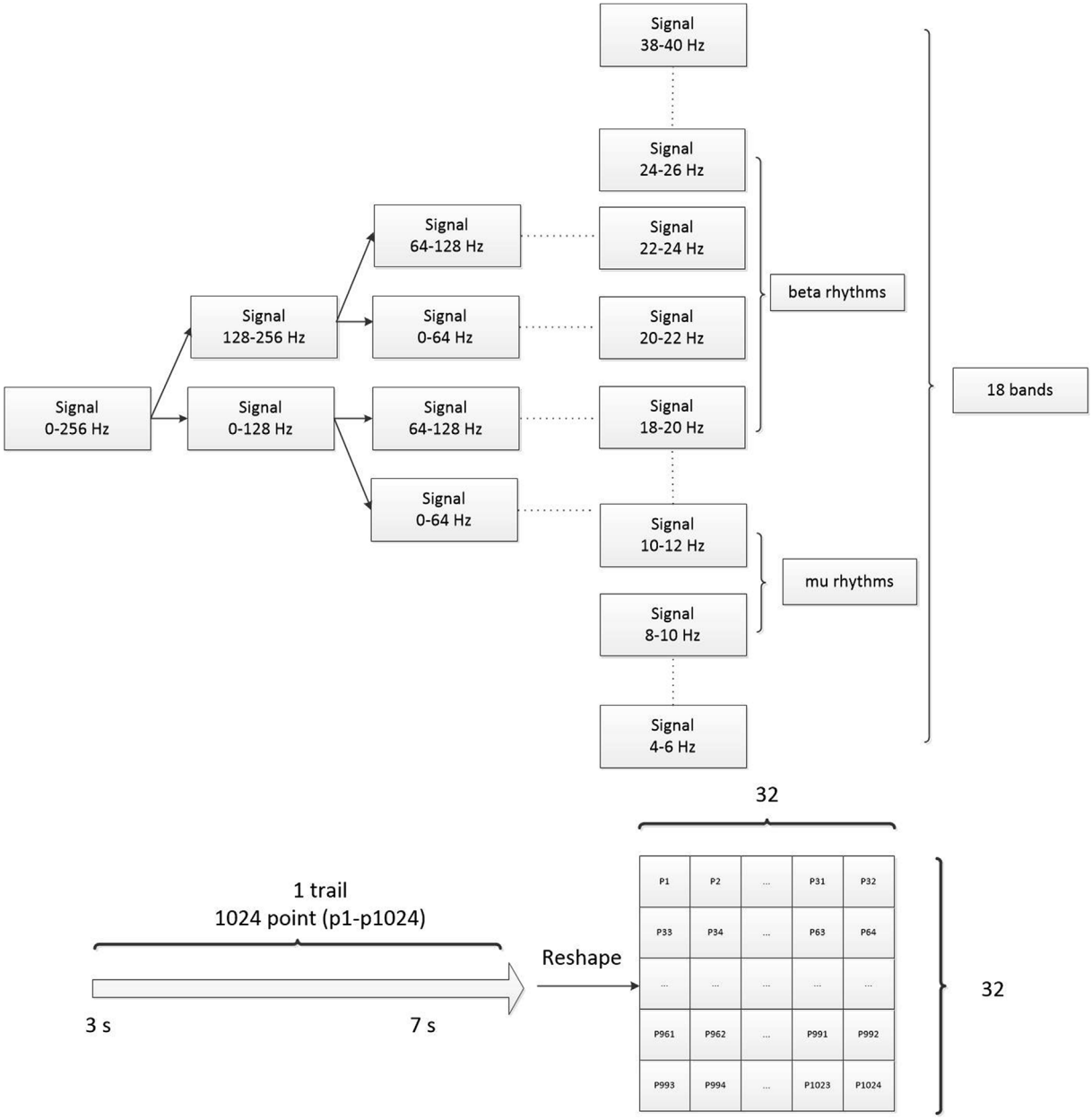

Fig. 5. Wavelet packet decomposition for EEG (top); reshape input feature (bottom).

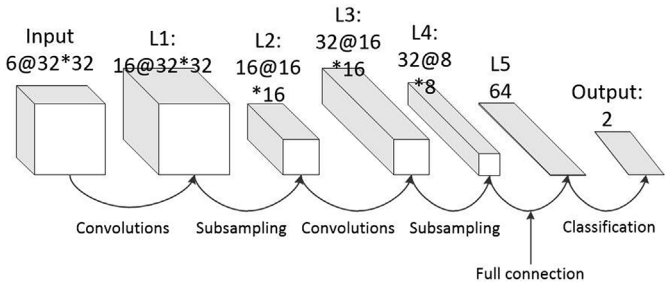

Fig. 6. Proposed convolutional neural network model.

the training, and 20% were selected for the testing set of each subject. We used ten-fold cross-validation for performance evaluation. We used the features and network described in Section 4. The network was trained by the batch normalization method [49,50]. Batch normalization was defined as

$$\mu = \frac{1}{m}\sum_{i=1}^{m} x_i \text{ batch mean} \tag{3}$$

$$\sigma^2 = \frac{1}{m}\sum_{i=1}^{m} (x_i - \mu)^2 \text{ batch variance} \tag{4}$$

$$\overline{x_i} = \frac{x_i - \mu}{\sqrt{\sigma^2 + \varepsilon}} \text{ normalize} \tag{5}$$

The accuracy results of the network methods are presented in Table 2 and Fig. 8. The average performance of each method over the subjects is also reported. We compared the performance of the SVM,k-NN, DBN and 2D CNN with the performance of 3D CNN for the same features. From these results, it can be clearly seen that the 3D CNN method is superior to the other methods for all subjects without S3 and S4. The average accuracy results of the 3D CNN methods were better than the other for the same features. moreover, for verify whether the performance difference between the proposed 3D CNN method and other methods is statistically significant, paired *t*-test has been

Table 1
Parameter of the CNN in each layer.

Layer	Filter	Size	Output	Activation	Number of parameters
L1	Conv	16@5*5	16@32*32	ReLU	(5*5 + 1)*16
L2	Sub-sample	2*2	16@16*16		
L3	Conv	32@5*5	32@16*16	ReLU	(5*5 + 1)*32
L4	Sub-sample	2*2	32@8*8		
L5	Full Con and Conv	Dropout-50% 64@8*8	32*8*8		(8*8*16 + 1)*64
L6	Output		2	Softmax	

conducted between the results of 3D CNN and other methods. The obtained p-values are given in Table 3. It show that all the obtained p-values are less than 0.05, which suggests that the performance improvement of 3D CNN over other methods is statistically significant (see Table 3).

The kappa results of our method are compared to current state-of-the-art studies in Table 4. Cohen's kappa coefficient (kappa) is a statistic that measures inter-rater agreement on qualitative items. It is generally thought to be a more robust measure than simple percentage agreement calculation, as kappa takes into account the possibility of the agreement occurring by chance. The definition of kappa is:

$$K = \frac{p_o - p_e}{1 - p_e} \quad (6)$$

where p_o is the relative observed agreement among raters (identical to accuracy), and p_e is the hypothetical probability of chance agreement (0.5) using the observed data to calculate the probability that any observer would randomly see each category. If the raters are in complete agreement, then k = 1. If there is no agreement among the raters other than what would be expected by chance, then K = 0. Table 3 shows that the SVM and k-NN approaches obtain a lower kappa coefficient than the CNN network approach. This means that the CNN method is more robust than other methods, and all results show that the CNN method provides better performance with higher accuracy.

5. Discussion

In this study, we purposed a portable EEG BCI. We used spring pin dry electrode, compared with micro-needle and soft conductive polymer electrode, our electrode was prepared easily, and has lower cost. The proposed dry electrodes could measure the EEG signals in hairy site. By the design of the proposed eletrodes, it effectively improves the convenience of use in daily life. Other studies have applied different wireless communication protocols, as shown in Table 5. These systems provide 16 channels or less, with typically less than 24-bit resolution per channel and a sampling rate less than 1000 SPS. The wireless modules used in these platforms communicates with Serial UART or SPI. These system dimensions are 5*5 cm. We proposed a system with a small size of 3*4 cm, which was attached to headphones.

Table 2
Accuracy for 3D CNN and other methods.

Subjects	Accuracy %				
	3D CNN	k-NN	SVM	DBN	2D CNN
S1	**81.7**	67.5	80.2	80.6	79.3
S2	**93.7**	70.7	85.1	89.2	86.5
S3	82.5	76.6	76.5	**82.6**	76.5
S4	62.2	50.6	67.2	60.2	**62.7**
S5	**74.3**	70.6	71.8	73.2	72.1
S6	**71.1**	62.5	66.2	70.1	67.8
S7	**82.1**	63.2	77.5	79.8	80.1
Average	**78.2**	65.8	74.9	76.5	75.0

Traditional BCI systems require the use of an EEG cap, however, the cap is uncomfortable, and the procedures usually create trouble for subjects. Thus, a headphone EEG was considered in the design of the proposed system. The subjects felt more comfortable with the headphones than with the EEG cap.

Fig. 9shows the event-related spectral perturbation (ERSP) results from the detection of MI on channels C3 and C4. ERSP is a 2D image of the average changes in the spectral power (dB) from a baseline. Calculating the ERSP typically requires computing the power spectrum over a sliding latency window.

The ERSP images were plotted using the EEGLAB toolbox. All of the no-green pixels of the ERSP images show significant (two-tailed permutation test, $P < 0.01$) post-stimulus increases or decreases from the spectral power compared with the pre-stimulus spectral power. The results were obtained from subjects 1 and 6 of offline experiments. Fig. 8 (a) shows that right-hand imagery tasks significantly decreased the alpha band and beta band after the stimulus for subject 1. An

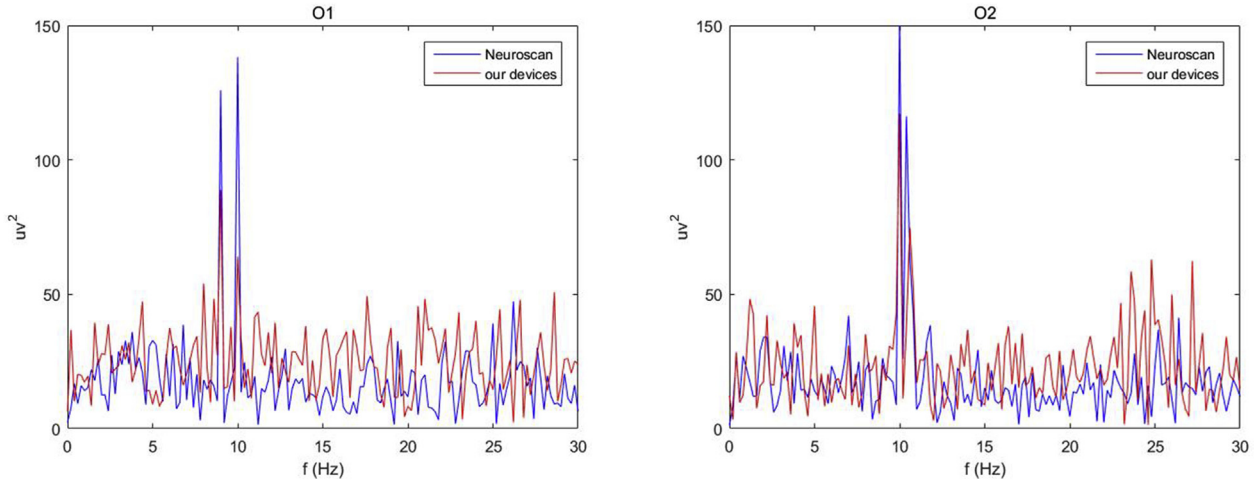

Fig. 7. Alpha wave detection from O1 and O2.

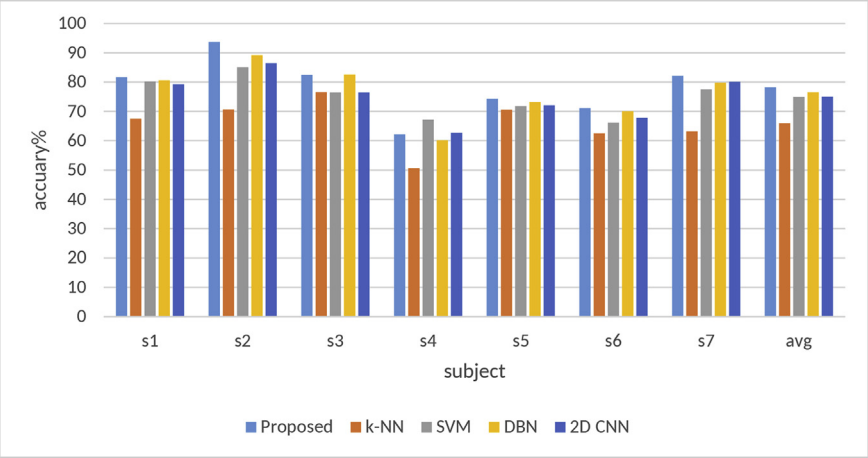

Fig. 8. Comparison of accuracy five methods.

Table 3
p-values of *t*-test between 3D CNN and other methods.

	k-NN	SVM	DBN	2D CNN
3D CNN	0.012	0.025	0.011	0.008

Table 4
Kappa value results for 3D CNN, and other methods.

Subjects	kappa				
	3D CNN	k-NN	SVM	DBN	2D CNN
S1	0.6340	0.3500	0.6040	0.612	0.586
S2	0.8740	0.4140	0.7020	0.784	0.730
S3	0.6500	0.5320	0.5300	0.652	0.530
S4	0.2440	0.1220	0.3440	0.204	0.254
S5	0.4860	0.4720	0.4360	0.464	0.442
S6	0.4220	0.4500	0.3240	0.402	0.356
S7	0.6420	0.2640	0.5500	0.596	0.602
Average	0.5645	0.3560	0.4981	0.530	0.500

increase in the power spectrum is shown by the ERS (red) 1000 ms after the stimulus in channel C3 for right-hand movement, while in C4, non-relevant variations appear. Fig. 8 (b) shows that ERD was not detected in the alpha band or the beta band. However, an ERS was clearly detected after 1000 ms. ERD/ERS activity in the alpha and beta band is often reported by scientific papers [54].

Several MI BCIs have been proposed in previous studies. Lo et al. proposed a wearable BCI with channel selection. Six EEG channels with dry electrodes were used for acquiring EEG signals, and several features were used for classifying MI. The accuracy was approximately 71%. Prakaksita et al. proposed a 14-channel EEG BCI based on Emotiv. The classification algorithms were ordinary neural network (NN) and optimized NN. The accuracy of the ordinary NN was 77%, and that for the optimized NN was 91% [55]. Cantillo-Negrete et al. proposed an eleven-channel EEG BCI to detect MI. The offline classification accuracy was 76 ± 7.6%, and the online accuracy was 70 ± 6.7% [56]. Jiang et al. proposed a semi-asynchronous wearable BCI. The subjects achieved a mean accuracy of 77.00% during MI tasks in the session with the highest accuracy [57].

The average accuracy for detecting MI in the proposed system was approximately 78.2%. The performance of the proposed system for detecting MI with only two EEG channels was similar to that of the above BCI systems. The proposed 3D CNN classification had better accuracy and a better kappa coefficient than the start-of-the-art methods. The performance improvement of 3D CNN over other methods is statistically significant.

The proposed system was also more comfortable for subjects compared to conventional wet electrodes and an EEG cap. There were no major complaints reported during the entire experiment. In another experiment, subjects provided a response (comfortable or not) related to wearing the proposed system and the EEG cap (Neuroscan). Most subjects reported that the EEG cap (Neuroscan) was painful after one hour of wear. Some subjects commented that they preferred the dry electrodes due to the improvement in user comfort.

6. Conclusion

The purpose of this study was to design and demonstrate a portable EEG BCI with 24 bit, analog-to-digital converters chip and wireless microprocessor unit. Novel CNN classification methods were found and used for offline and online experiments with a portable acquisition system. The system was experimentally validated for measuring EEG signals by an alpha wave experiment. The system has small size, excellent mobility, and low power consumption. We presented a novel classifier based on the 3D CNN. This classifier had better accuracy than state-of-the-art methods.

Our proposed BCI system consisted of nRF51822 (microprocessor

Table 5
Comparison of proposed system with existing systems.

Property	Proposed system	Pinho [51]	Campillo [52]	Myung [53]	Uktveris [48]
Dimension (cm)	3*4	13*11	7.5*10.5		10*5
Sampling (Hz)	1000	1000	500	512	1000
Resolution (bits)	24	24	12	24	24
CPU	nRF51822(BLE)	DM3730	MSP430	STM32	Atmega2560
IO	BLE 4.0	Wi-Fi 802.11	UART	Wi-Fi 802.11	BLE 4.0
CMRR	−110	−115	−94	–	−110
Gain	24	24	12	–	12
Local processing	No	Yes	No	No	No

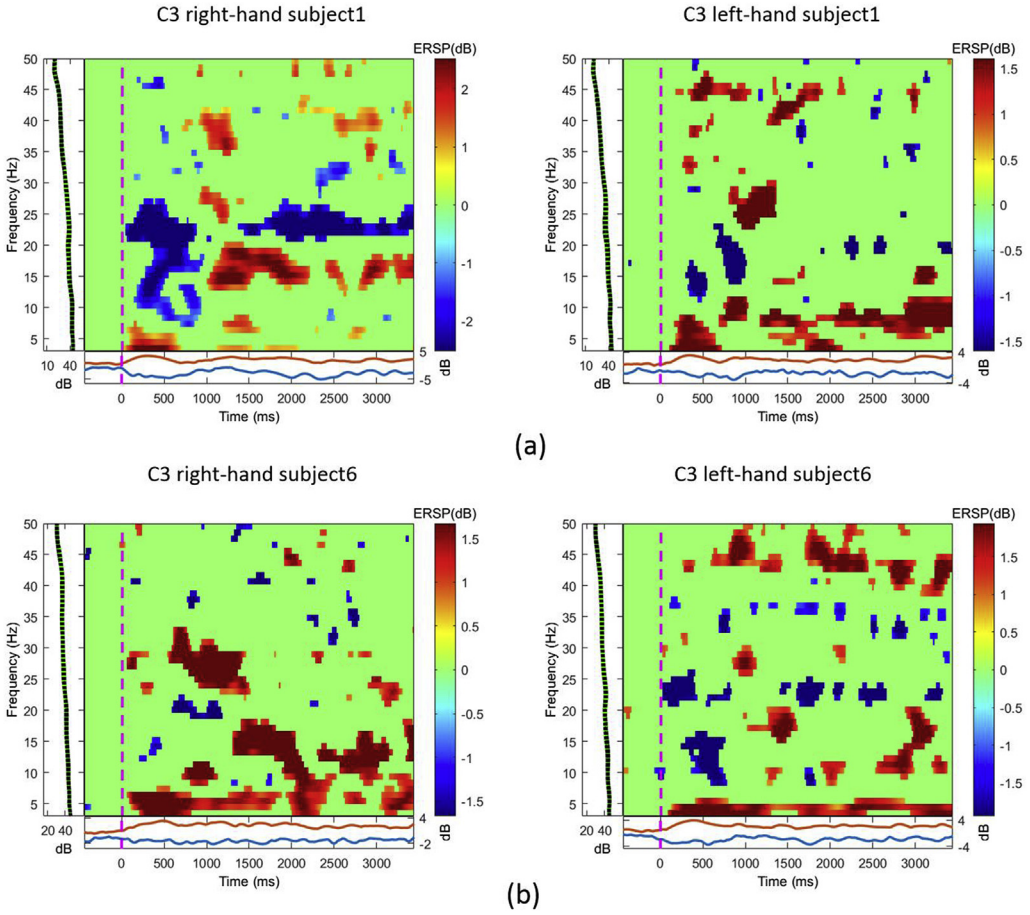

Fig. 9. ERSP from channel C3 for left-hand and right-hand imagery.

and Bluetooth) and ADS1298 (analog–digital conversion). This system had a small size (30*40 mm) and low power (200 mAh). The main difficulties with conventional BCIs are mobility and dry electrodes. In place of the dry electrode, we used a probe structure. Each probe consisted of head, spring, and sleeve. The head surface was gold-plated (Au), and the spring provided a force that acted as a buffer to maintain head–skin contact impedance. For mobility, our system had a small size, and was fixed on a headphone.

The alpha wave experiment suggests that this system has the potential to provide very stable EEG signals. Compared with the Neuroscan, our proposed system can acquire typical alpha waves in the occipital lobe area (O1 and O2) during an eyes-closed interval. This results is similar to Neuroscan.

We designed a novel classifier based on the CNN. This classifier had a different feature structure in the input layer. The signal was reshaped to a matrix in the time domain, and the third dimension was a different frequency band (channels@matrix ranks*matrix arrays). In the output layer, we used the dropout technique, and set the dropout probability to 50% to reduce overfitting. We believe this input model is more suitable for CNNs. In the MI experiments, the results demonstrate that CNN classification showed better accuracy and a better kappa coefficient than SVM or k-NN classification, the classification above 78% and kappa coefficient above 0.56. In the online experiments, we found that feedback could improve the classification accuracy of subjects with no experience.

Limitations and future work: although encouraging results were obtained from this study, there were several limitations. First, we only put electrodes on the headphone like line. In the MI experiment, C3 and C4 be used on central line. This device can't capture the frontal electrodes and central electrodes simultaneously. So it does not permit to assess the brain dynamics over the entire scalp. Second, the sample is not enough. Generally, the amount of data for deep learning is much larger than that. We think that the deep network maybe overfitting although we used dropout. So data augmentation maybe a solution.

Acknowledgments

It should be understood that none of the authors have any financial or scientific conflicts of interest with regard to the research described in this manuscript.

This work was supported by the National Key Research and Development Program of China (No. 2016YFB0401201), the National Science Foundation of China (No. 61505028), and Enterprises, Universities, and Research Institutes Prospective Joint Research Program of Jiangsu Province (No. BY2016076-07).

References

[1] D. Tan, A. Nijholt, Brain-computer interfaces and human-computer interaction, in: D.S. Tan, A. Nijholt (Eds.), Brain-Computer Interfaces: Applying our Minds to Human-Computer Interaction, Springer London, London, 2010, pp. 3–19.

[2] F. Lotte, et al., "A review of classification algorithms for EEG-based brain–computer interfaces: a 10 year update, J. Neural Eng. 15 (3) (2018) 031005.

[3] Chin-Teng Lin, Ruei-Cheng Wu, Sheng-Fu Liang, Wen-Hung Chao, Yu-Jie Chen, Tzyy-Ping Jung, EEG-based drowsiness estimation for safety driving using independent component analysis, IEEE Trans. Circuits Syst. Regul. Pap. 52 (12) (Dec. 2005) 2726–2738.

[4] A. Gevins, J. Le, N.K. Martin, P. Brickett, J. Desmond, B. Reutter, High resolution EEG: 124-channel recording, spatial deblurring and MRI integration methods, Electroencephalogr. Clin. Neurophysiol. 90 (5) (May 1994) 337–358.

[5] E. Moser, et al., Windows on the human body – in vivo high-field magnetic resonance research and applications in medicine and psychology, Sensors 10 (6) (Jun. 2010) 5724–5757.

[6] R. Matthews, N.J. McDonald, P. Hervieux, P.J. Turner, M.A. Steindorf, A Wearable

Physiological Sensor Suite for Unobtrusive Monitoring of Physiological and Cognitive State, 2007 29th Annual International Conference of the IEEE Engineering in Medicine and Biology Society, 2007, pp. 5276–5281.
[7] J.-C. Chiou, et al., Using novel MEMS EEG sensors in detecting drowsiness application, IEEE Biomedical Circuits and Systems Conference, vol. 2006, 2006, pp. 33–36.
[8] J.K. Radhakrishnan, S. Nithila, S.N. Kartik, T. Bhuvana, G.U. Kulkarni, U.K. Singh, A novel, needle-array dry-electrode with stainless steel micro-tips, for electroencephalography monitoring, J. Med. Devices 12 (4) (Sep. 2018) 041001-041001–7.
[9] L. Ren, et al., Fabrication of flexible microneedle array electrodes for wearable bio-signal recording, Sensors 18 (4) (Apr. 2018).
[10] L. Ren, et al., Flexible microneedle array electrode using magnetorheological drawing lithography for bio-signal monitoring, Sens. Actuators Phys. 268 (Dec. 2017) 38–45.
[11] Y.M. Chi, T.-P. Jung, G. Cauwenberghs, Dry-contact and noncontact biopotential electrodes: methodological review, IEEE Rev. Biomed. Eng. 3 (2010) 106–119.
[12] Y.M. Chi, G. Cauwenberghs, Wireless Non-contact EEG/ECG Electrodes for Body Sensor Networks, Wearable and Implantable Body Sensor Networks, International Workshop on(BSN), 2010, pp. 297–301.
[13] G. Gargiulo, P. Bifulco, R.A. Calvo, M. Cesarelli, C. Jin, A. van Schaik, A mobile EEG system with dry electrodes, IEEE Biomedical Circuits and Systems Conference, 2008, 2008, pp. 273–276.
[14] G. Gargiulo, et al., A new EEG recording system for passive dry electrodes, Clin. Neurophysiol. 121 (5) (May 2010) 686–693.
[15] S.L. Kappel, M.L. Rank, H.O. Toft, M. Andersen, P. Kidmose, Dry-contact electrode ear-EEG, IEEE Trans. Biomed. Eng. 66 (1) (Jan. 2019) 150–158.
[16] J.W.Y. Kam, et al., Systematic comparison between a wireless EEG system with dry electrodes and a wired EEG system with wet electrodes, Neuroimage 184 (Jan. 2019) 119–129.
[17] X. Xing, et al., A high-speed SSVEP-based BCI using dry EEG electrodes, Sci. Rep. 8 (1) (Oct. 2018) 14708.
[18] K.-P. Gao, H.-J. Yang, X.-L. Wang, B. Yang, J.-Q. Liu, Soft pin-shaped dry electrode with bristles for EEG signal measurements, Sens. Actuators Phys. 283 (Nov. 2018) 348–361.
[19] A. Subasi, M.I. Gursoy, EEG signal classification using PCA, ICA, LDA and support vector machines, Expert Syst. Appl. 37 (2010) 8659–8666.
[20] A. Yazdani, T. Ebrahimi, U. Hoffmann, Classification of EEG signals using Dempster Shafer theory and a k-nearest neighbor classifier, *2009 4th International IEEE/EMBS Conference on Neural Engineering*, Antalya, Turkey, 2009, pp. 327–330.
[21] H. Ramoser, J. Muller-Gerking, G. Pfurtscheller, Optimal spatial filtering of single trial EEG during imagined hand movement, IEEE Trans. Rehabil. Eng. 8 (4) (Dec. 2000) 441–446.
[22] V.J. Lawhern, A.J. Solon, N.R. Waytowich, S.M. Gordon, C.P. Hung, B.J. Lance, EEGNet: a compact convolutional network for EEG-based brain-computer interfaces, J. Neural Eng. 15 (5) (Oct. 2018) 056013.
[23] D. Krug, C.E. Elger, K. Lehnertz, "A CNN-based synchronization analysis for epileptic seizure prediction: inter- and intraindividual generalization properties, 2008 11th International Workshop on Cellular Neural Networks and Their Applications, 2008, pp. 92–95.
[24] L. Ma, J.W. Minett, T. Blu, W.S. Wang, Resting State EEG-based biometrics for individual identification using convolutional neural networks, 2015 37th Annual International Conference of the IEEE Engineering in Medicine and Biology Society, EMBC), 2015, pp. 2848–2851.
[25] I. Sturm, S. Lapuschkin, W. Samek, K.-R. Müller, Interpretable deep neural networks for single-trial EEG classification, J. Neurosci. Methods 274 (Dec. 2016) 141–145.
[26] R.T. Schirrmeister, et al., Deep learning with convolutional neural networks for EEG decoding and visualization, Hum. Brain Mapp. 38 (11) (2017) 5391–5420.
[27] N. Lu, T. Li, X. Ren, H. Miao, A deep learning scheme for motor imagery classification based on restricted Boltzmann machines, IEEE Trans. Neural Syst. Rehabil. Eng. 25 (6) (Jun. 2017) 566–576.
[28] Y. Lecun, L. Bottou, Y. Bengio, P. Haffner, Gradient-based learning applied to document recognition, Proc. IEEE 86 (11) (Nov. 1998) 2278–2324.
[29] A. Krizhevsky, I. Sutskever, G.E. Hinton, ImageNet classification with deep convolutional neural networks, in: F. Pereira, C.J.C. Burges, L. Bottou, K.Q. Weinberger (Eds.), Advances in Neural Information Processing Systems 25, Curran Associates, Inc., 2012, pp. 1097–1105.
[30] K. He, X. Zhang, S. Ren, J. Sun, Deep Residual Learning for Image Recognition, (Dec. 2015).
[31] P. Bashivan, I. Rish, M. Yeasin, N. Codella, Learning Representations from EEG with Deep Recurrent-Convolutional Neural Networks, (Nov. 2015) ArXiv151106448 Cs.
[32] H. Yang, S. Sakhavi, K.K. Ang, C. Guan, On the use of convolutional neural networks and augmented CSP features for multi-class motor imagery of EEG signals classification, Conf. Proc. Annu. Int. Conf. IEEE Eng. Med. Biol. Soc. IEEE Eng. Med. Biol. Soc. Annu. Conf. 2015 (2015) 2620–2623.
[33] L.G. Hernández, J.M. Antelis, A comparison of deep neural network algorithms for recognition of EEG motor imagery signals, Pattern Recognition, 2018, pp. 126–134.
[34] J. Yang, S. Yao, J. Wang, Deep fusion feature learning network for MI-EEG classification, IEEE Access 6 (2018) 79050–79059.
[35] A.M. Chiarelli, P. Croce, A. Merla, F. Zappasodi, Deep learning for hybrid EEG-fNIRS brain-computer interface: application to motor imagery classification, J. Neural Eng. 15 (3) (Jun. 2018) 036028.
[36] S. Sakhavi, C. Guan, S. Yan, Learning temporal information for brain-computer interface using convolutional neural networks, IEEE Trans. Neural Netw. Learn. Syst. 29 (11) (Nov. 2018) 5619–5629.
[37] H. Dose, J.S. Møller, H.K. Iversen, S. Puthusserypady, An end-to-end deep learning approach to MI-EEG signal classification for BCIs, Expert Syst. Appl. 114 (Dec. 2018) 532–542.
[38] Z. Tang, C. Li, S. Sun, Single-trial EEG classification of motor imagery using deep convolutional neural networks, Optik 130 (Feb. 2017) 11–18.
[39] Z. Wang, L. Cao, Z. Zhang, X. Gong, Y. Sun, H. Wang, Short time Fourier transformation and deep neural networks for motor imagery brain computer interface recognition, Concurrency Comput. Pract. Ex. 30 (23) (2018) e4413.
[40] Z. Tayeb, et al., Validating deep neural networks for online decoding of motor imagery movements from EEG signals, Sensors 19 (1) (Jan. 2019).
[41] J.D. Kropotov, Chapter 2.2 - alpha rhythms, in: J.D. Kropotov (Ed.), Functional Neuromarkers for Psychiatry, Academic Press, San Diego, 2016, pp. 89–105.
[42] W. Ting, Y. Guo-zheng, Y. Bang-hua, S. Hong, EEG feature extraction based on wavelet packet decomposition for brain computer interface, Measurement 41 (6) (Jul. 2008) 618–625.
[43] G. Pfurtscheller, F.H. Lopes da Silva, Event-related EEG/MEG synchronization and desynchronization: basic principles, Clin. Neurophysiol. 110 (11) (Nov. 1999) 1842–1857.
[44] Y. Kim, J. Ryu, K.K. Kim, C.C. Took, D.P. Mandic, C. Park, Motor imagery classification using mu and beta rhythms of EEG with strong uncorrelating transform based complex common spatial patterns, Comput. Intell. Neurosci. (2016) [Online]. Available: https://www.hindawi.com/journals/cin/2016/1489692/ , Accessed date: 18 September 2018.
[45] M. Tariq, L. Uhlenberg, P. Trivailo, K.S. Munir, M. Simic, Mu-beta rhythm ERD/ERS quantification for foot motor execution and imagery tasks in BCI applications, 2017 8th IEEE International Conference on Cognitive Infocommunications (CogInfoCom), Debrecen, 2017, pp. 000091–000096.
[46] M. Manjusha, R. Harikumar, Performance analysis of KNN classifier and K-means clustering for robust classification of epilepsy from EEG signals, 2016 International Conference on Wireless Communications, Signal Processing and Networking (WiSPNET), 2016, pp. 2412–2416.
[47] Y. Lin, C. Wang, T. Wu, S. Jeng, J. Chen, Support vector machine for EEG signal classification during listening to emotional music, IEEE 10th Workshop on Multimedia Signal Processing, vol. 2008, 2008, pp. 127–130.
[48] T. Uktveris, V. Jusas, Development of a modular board for EEG signal acquisition, Sensors 18 (7) (Jul. 2018).
[49] S. Ioffe, C. Szegedy, Batch normalization: accelerating deep network training by reducing internal covariate shift, (Feb. 2015).
[50] T. Cooijmans, N. Ballas, C. Laurent, Ç. Gülçehre, A. Courville, Recurrent batch normalization, (Mar. 2016).
[51] F. Pinho, J.H. Correia, N.J. Sousa, J.J. Cerqueira, N.S. Dias, Wireless and wearable eeg acquisition platform for ambulatory monitoring, IEEE 3nd International Conference on Serious Games and Applications for Health, vol. 2014, SeGAH), 2014, pp. 1–7.
[52] A real time ECG preprocessing system based on ADS1298 - IEEE Conference Publication, [Online]. Available: https://ieeexplore.ieee.org/document/6713535 , Accessed date: 11 October 2018.
[53] B.R. Myung, S.K. Yoo, Development of 16-channels compact EEG system using real-time high-speed wireless transmission, Engineering 05 (05) (2013) 93–97.
[54] G. Pfurtscheller, C. Brunner, A. Schlögl, F.H. Lopes da Silva, Mu rhythm (de)synchronization and EEG single-trial classification of different motor imagery tasks, Neuroimage 31 (1) (May 2006) 153–159.
[55] N. Prakaksita, C. Kuo, C. Kuo, Development of a motor imagery based brain-computer interface for humanoid robot control applications, *2016* IEEE International Conference on Industrial Technology (ICIT), 2016, pp. 1607–1613.
[56] J. Cantillo-Negrete, R.I. Carino-Escobar, P. Carrillo-Mora, D. Elias-Vinas, J. Gutierrez-Martinez, Motor imagery-based brain-computer interface coupled to a robotic hand orthosis aimed for neurorehabilitation of stroke patients, Journal of Healthcare Engineering (2018) [Online]. Available: https://www.hindawi.com/journals/jhe/2018/1624637/ , Accessed date: 17 October 2018.
[57] Y. Jiang, N.T. Hau, W. Chung, Semiasynchronous BCI using wearable two-channel EEG, IEEE Trans. Cogn. Dev. Syst. 10 (3) (Sep. 2018) 681–686.